ARTICLE   OPEN

Check for updates

Forest canopy mitigates soil N$_2$O emission during hot moments

Ülo Mander [1,2✉], Alisa Krasnova [1,3], Jordi Escuer-Gatius [3], Mikk Espenberg [1], Thomas Schindler [1,2], Katerina Machacova [2], Jaan Pärn [1], Martin Maddison [1], J. Patrick Megonigal [4], Mari Pihlatie [5,6,7], Kuno Kasak [1], Ülo Niinemets [3], Heikki Junninen [8] and Kaido Soosaar [1,2]

Riparian forests are known as hot spots of nitrogen cycling in landscapes. Climate warming speeds up the cycle. Here we present results from a multi-annual high temporal-frequency study of soil, stem, and ecosystem (eddy covariance) fluxes of N$_2$O from a typical riparian forest in Europe. Hot moments (extreme events of N$_2$O emission) lasted a quarter of the study period but contributed more than half of soil fluxes. We demonstrate that high soil emissions of N$_2$O do not escape the ecosystem but are processed in the canopy. Rapid water content change across intermediate soil moisture was a major determinant of elevated soil emissions in spring. The freeze-thaw period is another hot moment. However, according to the eddy covariance measurements, the riparian forest is a modest source of N$_2$O. We propose photochemical reactions and dissolution in canopy-space water as reduction mechanisms.

INTRODUCTION

The role of forests in regulating greenhouse gas (GHG)[1] budget, in particular for nitrous oxide (N$_2$O), is still largely unknown[2]. The increase in atmospheric N$_2$O levels from a pre-industrial concentration of 270 ppbv to 328 ppbv in 2016[3] is of concern because: (i) N$_2$O is responsible for approximately 6% of global radiative forcing from anthropogenic GHGs, (ii) N$_2$O is the ruling stratospheric ozone-layer depleting agent in the 21st century[4], and (iii) N$_2$O the third most important GHG with a global warming potential 296 times that of CO$_2$[3] (100-year lifetime adjustment, with feedbacks). A variety of nitrogen cycle processes can produce N$_2$O[5] but in riparian soils, denitrification is the most important source of N$_2$O[6].

Hot spots and hot moments (extreme emission events) largely determine spatio-temporal variation of N$_2$O emissions from soils[7], and soil volumetric water content (SWC) is a leading factor controlling hot moments. An SWC value of 0.5–0.8 m^3 m^{-3} has been shown to be optimal for soil N$_2$O emissions in forests on both mineral soils[8] and organic soils[9]. Therefore, depending on the initial moisture, both flooding and drought can induce hot moments in forests[10]. Drought decreases soil N$_2$O emissions or even turns the soil into a sink of N$_2$O[11]. Another mechanism that creates hot moments of soil N$_2$O emission is freeze-thaw cycles[12–15]. Although there are several hypotheses explaining the impact of freeze-thaw cycles on soil N$_2$O emissions[14,16,17], a generally accepted theory of the impact of freeze-thaw on N$_2$O fluxes is still missing.

Besides soils, plants including trees are known to exchange N$_2$O with the atmosphere[18–21]. N$_2$O emitted from tree stems and canopy may originate from the soil[18,19], from microbial or fungal activity within the tree stem, or from plant biophysical processes[21]. The relative contributions of these sources to N$_2$O exchange between stems and the atmosphere is unclear in any

tree species, including Gray alder (*Alnus incana*), a common species in riparian areas that are widespread across the Northern Hemisphere[22] (Supplementary Fig. 1).

Above tree canopies, long-term ecosystem-level N$_2$O flux measurements using the eddy covariance (EC) technology are still scarce[23–25]. No previous complex investigations on forest ecosystems' N$_2$O budgets (soil and tree stem flux studies with EC measurements above the canopy) exist.
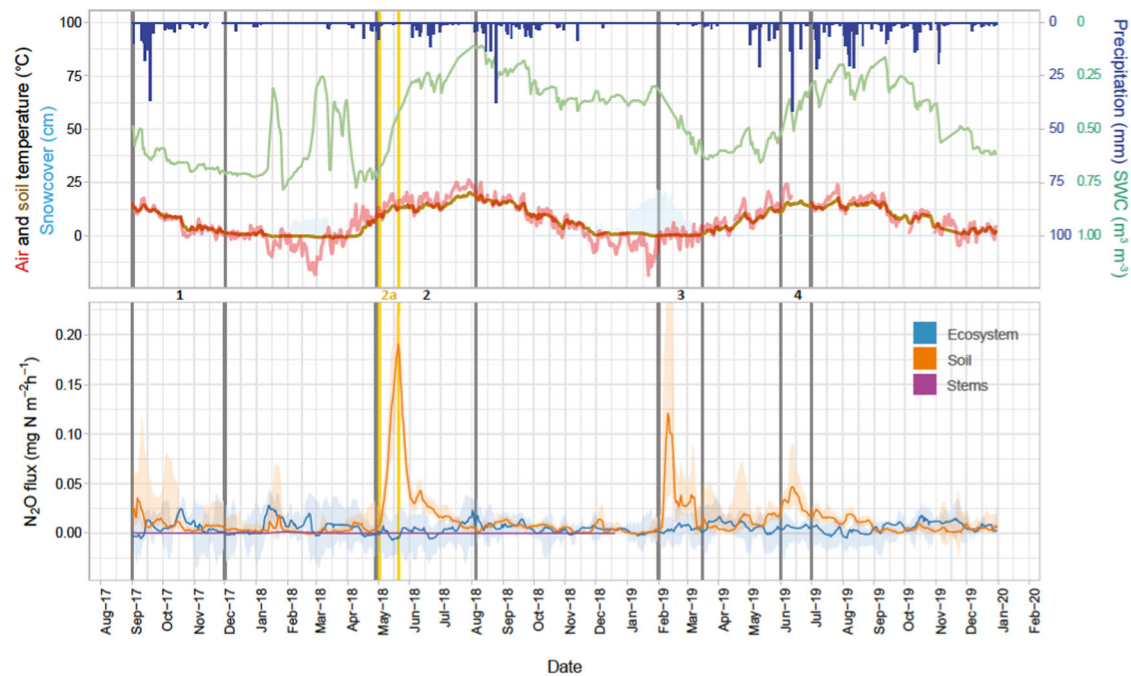
We analyze 2.5-years seasonal and interannual dynamics of N$_2$O fluxes in a deciduous riparian forest using high temporal frequency measurements made at the scale of the whole ecosystem and from two ecosystem components, soils and tree stems. We relate the fluxes to key environmental factors to test the following hypotheses: (1) soil water content (SWC)- and temperature-related hot moments determine long-term patterns of N$_2$O fluxes, and (2) EC-measured N$_2$O fluxes are coherent with the sum of soil and stem fluxes.

RESULTS

Soil N$_2$O fluxes

Across the study period, the soil N$_2$O fluxes were highly dynamic, with the annual budget largely driven by the short-lived hot moments (Fig. 1 and Supplementary Fig. 2). N$_2$O fluxes varied from −0.040 to 1.50 mg N m^{-2} h^{-1} while daily averages reached 0.225 mg N m^{-2} h^{-1} (Fig. 2). The heatmap in Supplementary Fig. 3 presents a spatial and temporal variation of these values, showing that across the whole study period, no remarkable difference between the values was measured in individual chambers. Negative N$_2$O fluxes occurred primarily in winter months when the near-ground air temperature was consistently negative, accounting for 43% of monthly values in February 2018 and January 2019

Fig. 1   Dynamics of ecosystem-level N₂O fluxes in the Agali gray alder forest during the study period Sep 2017–Dec 2019. Lines are 5-day median values and shaded areas are 25th and 75th percentiles. Vertical lines show the beginning and end of hot moments: 1 = Wet (2017-09-01 … 2017-12-01), 2 = Dry (2018-05-01 … 2018-08-05) with 2a = Drought Onset (2018-05-02 … 2018-05-21), 3 = freeze-thaw (2019-02-01 … 2019-03-15), and 4 = Dry-Minor (2019-06-01 … 2019-06-30). The air temperature was measured at 50 cm from the soil surface representing the near-ground air temperature. Note that the origins are on opposite ends of the left- and right-side axes.

(Supplementary Fig. 4). We identified four hot moments in soil N₂O flux time series defined by remarkably higher flux values (Fig. 1). The highest flux values (>0.10 mg N₂O–N m^{-2} h^{-1}) were observed during the Drought Onset period starting in May 2018, accounting for a maximum of 38% of the measurements (Supplementary Fig. 3). During this short period, the daily average flux in all individual chambers was >0.02 mg N m^{-2} h^{-1} (Supplementary Fig. 3). The freeze-thaw period in 2019 contributed 14% of the whole soil emission (Supplementary Table 1). We attribute the absence of a freeze-thaw hot moment in 2018 to consistently negative near-ground air temperature and stable (2–12 cm deep) snow cover in January and February 2018 (Fig. 1) that would impede N₂O diffusion rates.

During the whole study period (September 2017–December 2019) the cumulative N₂O soil flux was 458.8 ± 7.7 mg N m^{-2} (mean ± standard error, SE) and the hot moments contributed 56% of the whole flux (Supplementary Table 1). During the calendar years 2018 and 2019, 196.3 ± 7.1 and 221.0 ± 12.4 mg N m^{-2} year^{-1} were emitted as N₂O (Supplementary Table 1). Considering the two full years of the study (September 2017–September 2018 and September 2018–September 2019), the corresponding cumulative flux values were 215.5 ± 7.7 and 221.4 ± 12.2 mg N m^{-2} year^{-1} (Fig. 3; Supplementary Table 2)

Except for the dry hot moments, we found no remarkable diurnal pattern of soil N₂O fluxes. Average day-time values during the dry hot moment were up to 100 times higher than those in the night-time showing that the variability was higher than in the other months (Supplementary Fig. 5).

Stem N₂O fluxes

Stem fluxes of N₂O measured during 52 campaigns averaged over all measured heights and expressed per m² of soil surface varied between −0.00028 and 0.0228 mg N m^{-2} h^{-1}. The highest emissions were measured on the lowest position of tree stems whereas

at higher positions (170 cm aboveground) slight consumption was observed. Stem flux during the measurement period from September 2017 to December 2018 was 0.00022 ± 0.00007 mg N₂O–N m^{-2} h^{-1} (mean ± SE). The wet and dry hot moments contributed respectively 41% and 12% of total cumulative emissions during the whole stem measurement period (3.53 mg N m^{-2}; Supplementary Table 1; Fig. 3).

Ecosystem level N₂O fluxes

The daily sums of ecosystem N₂O fluxes varied relatively little, ranging from −0.60 to 1.16 mg N m^{-2} d^{-1}. Of the whole measurement period, 76% passed the quality check and we gap-filled the remaining 24% (Fig. 4). Hot moments of soil N₂O fluxes were not reflected at the ecosystem scale (Figs. 1 and 3), but showed a seasonal pattern of high positive fluxes in spring (March–April) and autumn months (October–November) and small fluxes near zero over summer months (Figs. 4 and S6). Likewise, higher values were observed during the "Wet" hot moment with 22% of the total cumulative EC flux of the whole study period (78.2 mg N m^{-2}; Figs. 3 and 4, Supplementary Table 1). We observed a distinctive diurnal pattern with small negative fluxes during the morning hours (8 a.m. to 12 a.m.) in the summer months of both years. We observed no diurnal pattern in either the simultaneous soil fluxes or in EC fluxes of autumn, winter, or spring months. The hourly average EC flux values ranged from −0.05 to 0.03 mg N₂O–N m^{-2} h^{-1} (Supplementary Fig. 4).

Relationships between N₂O flux and environmental parameters

The main factors related to N₂O soil fluxes in this riparian forest ecosystem were SWC and soil temperature (Fig. 2a). Based on the full data set measured during the study period, there was an optimal SWC value of about 0.5 m³ m^{-3} at which the soil flux was the highest (Fig. 2b). The relationship between the soil surface
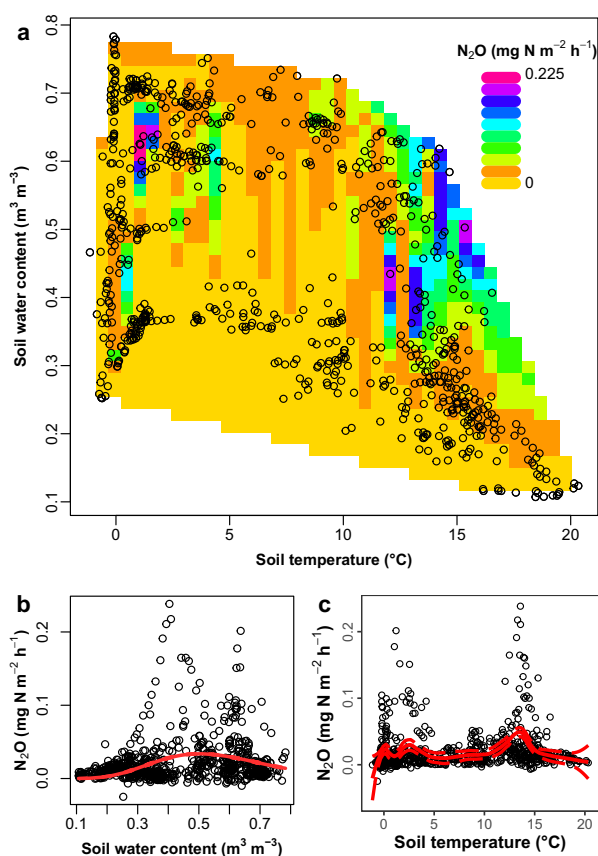
Fig. 2 Relationships between the soil temperature, soil water content (SWC), and flux of N_2O from the soil over the study period. **a** Contour plot showing relationships between soil temperature, SWC, and N_2O emission ($n = 755$). **b** Regression curve of SWC vs. N_2O fluxes. Curve fitted regression of SWC and N_2O flux ($R^2 = 0.07$, $p < 0.01$, $n = 757$). $N_2O = (15725.05 \times SWC^{7.73}) \times \exp(-15.38 \times SWC)$. **c** Regression curve of soil temperature vs N_2O. Local polynomial regression fitting of soil temperature and N_2O flux ($R_2 = 0.13$, $p < 0.01$, $n = 756$). The dashed red lines represent 95% confidence intervals for the regression line.

temperature and soil N_2O flux was more complex showing two peaks, one at 0–4 °C and a second one at 13–14 °C (Fig. 2c). The first peak corresponds to the freeze-thaw hot moment and the second one represents the dry and dry-minor hot moments.

During the Dry hot moment, the correlation between the SWC and soil N_2O emission was very strong, showing a clear peak at SWC values between 0.35 and 0.5 m³ m⁻³ (Fig. 5).

We did not find any significant relationships between ecosystem N_2O fluxes and environmental parameters (air temperature, soil temperature, SWC, wind speed) or gross primary production (GPP) on the half-hourly scale. However, weekly average fluxes followed the same general pattern as that of SWC with the modifying influence of changes in air temperature (Supplementary Fig. 6). The stem N_2O fluxes were also related to SWC with a positive but insignificant correlation ($p = 0.09$) while no clear relationship was found during the hot moments.

Comparing the monthly average soil and EC fluxes of N_2O to weather patterns, we found that during the spring (drought onset and end of freeze-thaw periods) the largest differences between the soil and EC fluxes coincided with the largest percentage of clear days (cloudiness ratio <0.4; Fig. 6). Differences between the soil and EC fluxes were lowest during the autumn and winter with the highest number of days of potential fog formation (dew point depression (DPD) < 4 °C) (Fig. 6).
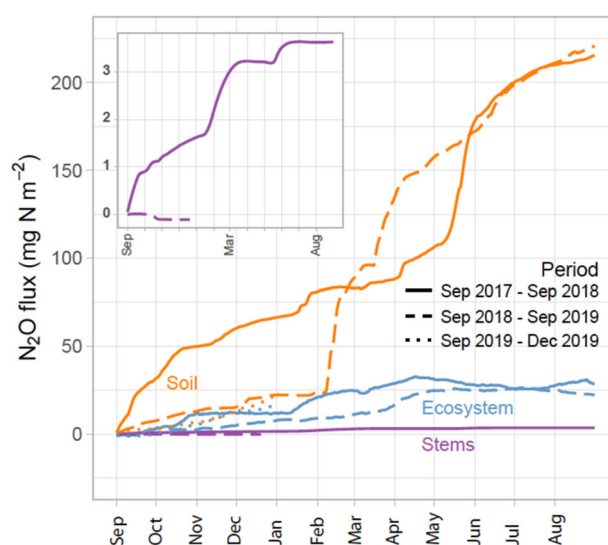
Fig. 3 Cumulative fluxes of N_2O from the soil, stems, and the ecosystem (eddy covariance above the canopies). Data from two full years (September 2017–September 2019) and one half-year (September–December 2019). Due to significantly lower values, the stem fluxes are also plotted in the inset. Notice that the stem fluxes have been measured from Sept 2017 to Dec 2018.

DISCUSSION

We hypothesized that SWC was the main factor associated with hot moments of N_2O emission from a riparian forest ecosystem. Our data generally supported this hypothesis for soil emissions, but we suggest that drought and rewetting triggered these events by different mechanisms as previously argued[26]. We identified four periods during which N_2O hot moments arose due to distinct mechanisms (Figs. 1 and 2). Across all cases, N_2O fluxes peaked at SWC value around 0.5 m³ m⁻³.

Soil N_2O emissions during the dry and freeze-thaw hot moments were 8–10 times higher than the period averages (Supplementary Fig. 2). N_2O emissions from intact soil mesocosms from a temperate forest showed an increase of up to four orders of magnitude following flooding pulses[27], consistent with the effects of fluctuating groundwater table depth on N_2O emissions under field conditions[28].

The highest soil N_2O fluxes in the present study were observed at SWC values around 0.5 m³ m⁻³ (Fig. 2b), a pattern that was most dramatic during drought onset (Fig. 5). Although several studies have shown a similar relationship[8,9], the direction of change in soil N_2O emissions depends on whether the soil is initially dry (SWC < 0.45 m³ m⁻³) or wet (SWC > 0.45 m³ m⁻³). Drought has been shown to decrease N_2O emissions in dry mineral soils[15], but increase N_2O emissions in wet soils (SWC > 0.6 m³ m⁻³)[9,29]. We observed both trends: a substantial drought-driven increase of N_2O emissions under wet conditions (SWC > 0.7 m³ m⁻³; Drought Onset episode) and a drought-driven decrease of N_2O emissions in dry conditions (SWC < 0.45 m³ m⁻³; end of dry period) with short-term emission peaks caused by precipitation-driven rewetting (dry-minor period; Supplementary Fig. 2). In all cases, the highest emissions occurred when the SWC transitioned past an optimum value of about 0.5 m³ m⁻³ (Supplementary Fig. 2).

During the freeze-thaw period, a different complex set of factors caused a substantial increase in soil N_2O emissions. Several hypotheses have been posed to explain this phenomenon, the most common of which are: (i) disruption of soil aggregates exposing physically protected organic matter to rapid mineralization by microorganisms[14]; (ii) the death of microorganisms, fine roots, and mycorrhiza during the freeze[16], providing rapidly decomposable organic matter for the thaw; and (iii) the death of
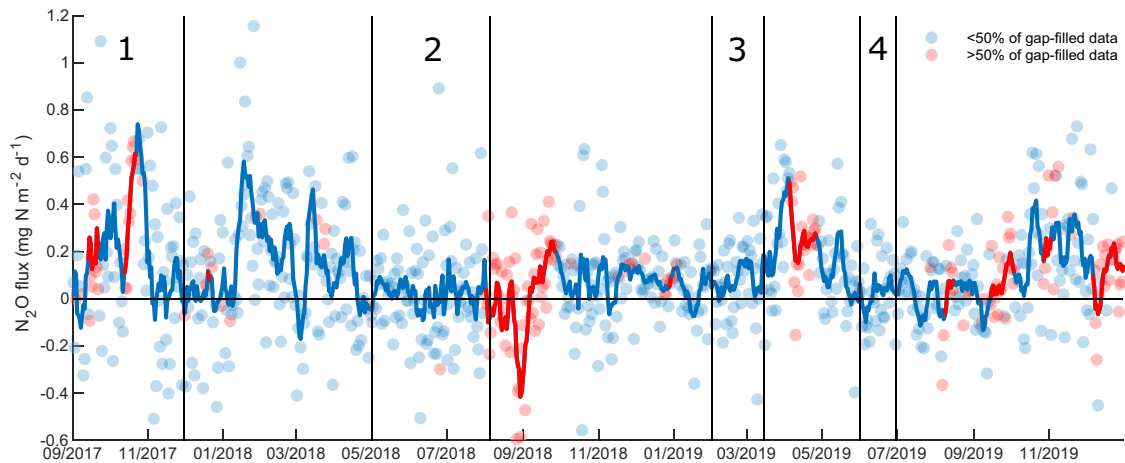
Fig. 4 Seasonal cycle of ecosystem N$_2$O flux measured with quantum cascade laser absorption spectrometer in eddy tower. The markers denote daily total values, the line is a 7-day running mean. The periods marked with red color represent time intervals with gap-filled data (MDS-method) exceeding 50%. Hot moments: 1—wet, 2—drought (without showing drought onset), 3—freeze-thaw, and 4—dry-minor.
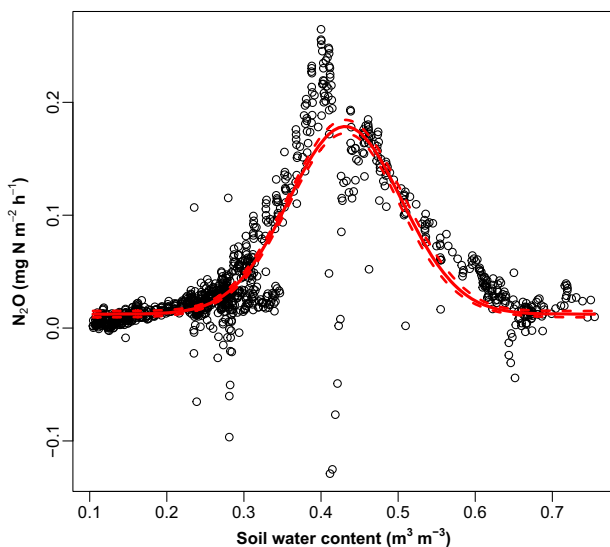
Fig. 5 Dynamics of soil water content (SWC) vs soil N$_2$O flux (hourly average values) during the dry hot moment (2018-05-01 ... 2018-08-05). The curve is calculated after the Bragg equation with four parameters: $Y = c + (d - c) \times \exp(-b) \times (X - e)^2$, where $b = 92.77$, $c = 0.0123$, $d = 0.1786$, $e = 0.4314$ and X is SWC and Y is N$_2$O flux ($R^2 = 0.74$, $p < 0.001$, $n = 1065$).

fine roots decreasing competition between roots and microorganisms for nitrate, the main substrate for N$_2$O production[16]. However, the underlying mechanism involved in the pulse emissions of N$_2$O remains uncertain and further exploration is required[30]. In addition, rising SWC played a role in N$_2$O fluxes at the end of the freeze-thaw (Supplementary Fig. 3), similarly to the observations of Öquist et al.[31].

The different hot moment mechanisms were driven by different relationships with the environmental factors. During the drought onset, there was a strong negative correlation ($R_{Spearman} = -0.93$) between the speed of SWC decrease and N$_2$O flux (Supplementary Fig. 7a). Only a few authors have considered drying speed as a factor in soil nitrogen cycle processes[32–34] and we report the phenomenon in situ. Accordingly, the speed of SWC decrease could be included in N$_2$O flux models. This resonates with the review by Barrat et al.[26] showing that the bigger the increase in SWC the larger the N$_2$O pulse. In our freeze-thaw period, a positive correlation ($R_{Spearman} = 0.64$) between the near-floor air

temperature and N$_2$O flux was observed (Supplementary Fig. 7b) suggesting that temperature may play a dominant role in the initiation of the hot moments. Likely, after the freeze, which physically breaks soil organic matter, and releases nutrients and dead microbial biomass, an increase in temperature stimulate microbial activity. This is fed by the newly released carbon and nitrogen to form N$_2$O peaks. Indeed, we did not observe meaningful diurnal patterns in soil N$_2$O fluxes during most of the study period, except for the dry and freeze-thaw hot moments (Supplementary Fig. 4). Until now only a few studies on terrestrial ecosystems have reported differences in soil N$_2$O emissions between day and night[35].

The second hypothesis that EC-measured N$_2$O fluxes are coherent with the sum of soil and stem fluxes was not supported. The ecosystem N$_2$O flux measured by the EC technique above the forest canopy was relatively low and did not follow the variability in soil N$_2$O fluxes (Figs. 1, 2, and 4). During the wet period, one significant N$_2$O peak was observed, while emissions remained low during the rest of the period. Other hot moments of soil N$_2$O flux did not increase ecosystem N$_2$O flux (Fig. 4, Supplementary Figs. 2 and 8). The cumulative N$_2$O emission from the ecosystem (78.2 mg N m^{-2}) was 5.9 times smaller than the soil's emission (458.8 mg N m^{-2}; Supplementary Table 1; Fig. 3). During the 1.5 years, the cumulative flux from alder stems was 3.53 mg N m^{-2}, which constituted only 0.8% of cumulative soil fluxes (Supplementary Table 1).

Because the measurement frequency was sufficient to capture all the fluxes above the canopy it is difficult to explain such a large difference between the soil and ecosystem emissions. We offer the following explanations of this difference:

(1) Horizontal advective fluxes and decoupling of gas fluxes between the layers are likely important reasons. While our study site is located on flat terrain, below-canopy horizontal advection could still play a role, especially in a closed canopy forest ecosystem. Dense canopies can reduce vertical mixing and decouple the layers below and above the canopy[36] in a way that peaks of soil N$_2$O emissions leak horizontally undetected by the EC system. For instance, during the Drought Onset episode in 2019, N$_2$O mixed ratios increased during wind-still nights (Supplementary Fig. 8) undetected by the EC measurements. Probably, a combination of poor mixing of soil-borne N$_2$O during low friction velocity ($u*$) and wind speed and decoupling of soil-borne and above canopy N$_2$O flux measurements due to the dense canopy layer
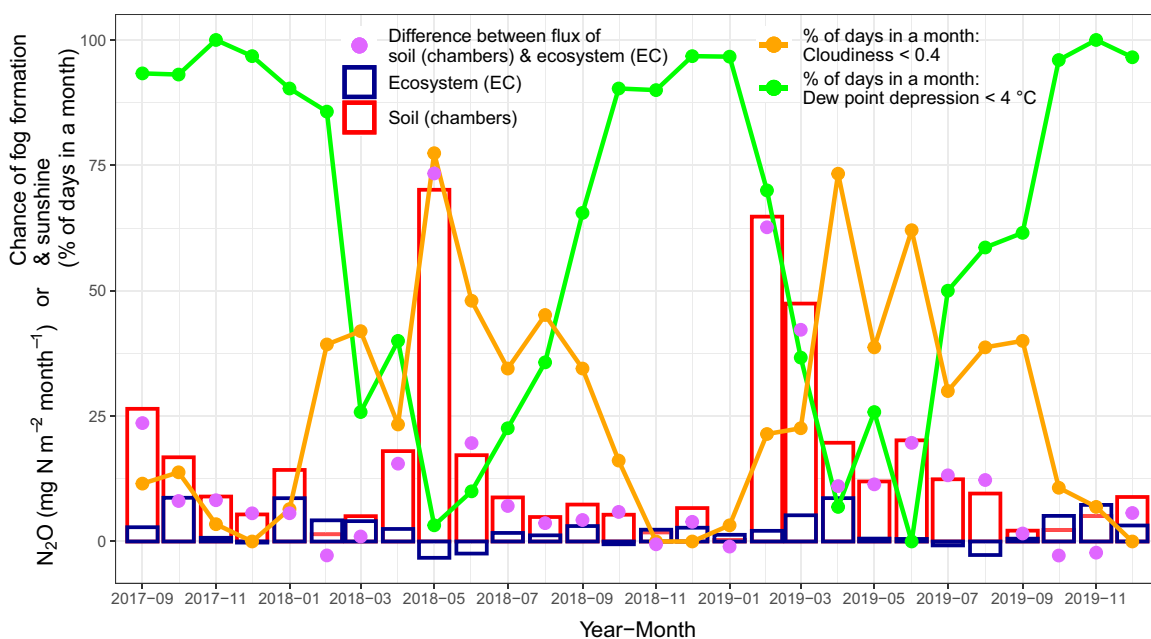
Fig. 6 N₂O fluxes (soil and eddy covariance) related to the chance of sunshine and fog formation. Relationship between the monthly sum of soil and EC fluxes of N_2O (mg N m^{-2} month^{-1}) with the percentage of days with a high chance of sunshine (cloudiness ratio <0.4) and fog formation (dew point depression <4 °C). During the drought onset (May 2018) and dry-minor (June–July 2019) periods photochemical reactions might play an important role in decreasing ecosystem (EC) flux of N_2O, whereas during the Wet (September–November 2017) and freeze-thaw (February 2019) periods absorption on wet surfaces and water droplets could be the reason for the decrease in EC N_2O flux. The difference between the soil and EC N_2O fluxes is negatively correlated with the percentage of days in a month with dew point depression <4 °C, whereas a positive trend is observed both in the difference between soil and EC flux and the share of sunny days (cloudiness ratio < 0.4) in a month.

(Supplementary Fig. 8). Nevertheless, the absence of concentration profile measurements and our simplified approach to the storage calculation may have contributed to the discrepancy between the soil chamber and EC measurements.

(2) UV-induced photodissociation may play a role in decreasing N_2O flux above the canopy. Typically for the drought onset episode, EC fluxes declined during the clear sunny days (Supplementary Fig. 4b). Thus, reduction during daylight could be explained by the UV-induced photodissociation of N_2O as found in other ecosystems[37]. Indeed, UV-induced N_2O photolysis is included as an important process in the assessment of the atmospheric lifetime of N_2O[38]. In our study, the monthly sum of sunshine hours was highest during the drought onset and dry-minor episodes when the differences between the soil and EC fluxes of N_2O were large (Fig. 6; Supplementary Fig. 9). During the dry period from May to August 2018, midday UV-B radiation of 295–315 nm wavelength was consistently 1–1.5 W m^{-2} (unpublished data from the nearby SMEAR Estonia station), up to 6 times higher than the cloudless noon values measured in Scandinavia by Fraser et al.[39] and in 2016 in our study area[40]. Thus, during the dry and dry-minor episodes, photochemical reactions may have decreased the ecosystem (EC) flux of N_2O measured above the canopy. On the other hand, the canopy shelter could mitigate the effect of UV radiation and increase the N_2O concentration within the canopy. This again proves the need for profile measurements in such studies.

(3) Potential N_2O dissolution in atmospheric water. In autumn, winter, and spring the consumption of N_2O could be related to the high solubility of N_2O gas in water (1.0 ml gas per ml water at 5 °C)[41]. For example, Warneke et al.[42] reported that absorption of N_2O in woodland soil water contributed up to half of the total N_2O consumption in the soil. In the present case, part of the N_2O produced during the freeze-thaw period may have been absorbed in fog. Eugster et al.[24] in their early

EC study in a mixed forest suggested that wetting of the canopy in fog can have a strong influence on N_2O fluxes; however, no clear evidence of absorption in fog has been reported. Likewise, Min et al.[43] found that NOx fluxes from the forest canopy were smaller than measured soil NOx emissions and referred to the phenomenon as a "canopy reduction factor" which they applied to soil NOx emissions in large-scale models. The interpretation of these differences was a chemical conversion of NOx to other nitrogen oxides within the forest canopy. Fulgham et al.[44] report that wet surfaces of leaves, needles, and branches in a mixed forest control the vertical exchange of volatile organic acids. The exchange velocity of these gases was well correlated with DPD. This is compatible with our findings on the difference between the soil and EC fluxes during the freeze-thaw period with high DPD (Fig. 6; Supplementary Figs. 9 and 10). We speculate that some of the soil-emitted N_2O is absorbed in the water droplets and films on soil, stem, and leaf surfaces, hence removing N_2O from the air. From the canopy, dissolved N_2O can be transported to soils via stemflow and throughfall[45]. We also observed either correspondence or a couple-week difference between the dynamics of N_2O EC flux and the peaks of its possible regulator—the maximum potential concentration of dissolved N_2O in m³ of air calculated based on LiCor-measured water vapor at EC tower (Supplementary Fig. 11).

It is difficult to evaluate the relative importance of these non-exclusive causes of the discrepancy between the soil, stem, and ecosystem fluxes of N_2O with the present data set. In addition to the soil and tree stem measurements made in this riparian forest, a better understanding of forest N_2O budgets also require the canopy-, and leaf-level measurements as well as assessment of advective flux and storage by profile measurements[24,46].

Comparison of our results with other studies is hampered by the fact that almost all previously reported annual rates of N_2O

emissions from forests are based on soil surface measurements only. Our alder soil surface emitted an average of 2.18 kg N ha^{-1} year^{-1} (average for the period Sept 2017–Sept 2019; Supplementary Table 2) similar to the IPCC emission factors for the boreal drained nutrient-rich forest on organic soil[47] (3.2 kg N ha^{-1} year^{-1}) and temperate drained forests on organic soil[47] (the 2.8 kg N ha^{-1} year^{-1}), but several times less than from peatlands drained for agriculture[48] or other drained N-rich peatlands[9]. However, based on our whole-ecosystem EC data we found that above-canopy N$_2$O emissions are an order of magnitude less (0.35 kg N ha^{-1} year^{-1}; Supplementary Table 2) than the soil estimates. This implies an 84% overestimate of soil-based emission estimates for temperate drained forests on organic soils.

Gray alder (*Alnus incana*) forests are widely distributed in Europe and North America[22] (Supplementary Fig. 1), often dominating riparian forest communities[49]. Upscaling our N$_2$O flux values to the whole *Alnus incana* subsp *incana* distribution area in Europe (15,000 km^2)[22], we estimate total annual emissions of 3270 (soil-based) or 390 tons (forest ecosystem-based) of *N* a year. Thus, in addition to several ecosystem services which riparian alder forests can provide, they are low emitters of N$_2$O and therefore attractive for riparian zone management when considering climate impacts.

The outcomes of our 2.5-years study show that this alder forest is a weak net source of N$_2$O. Hot moments related to SWC and temperature accounted for 56% of soil emissions throughout the whole study period. The soil N$_2$O flux peaked at about 0.5 m^3 m^{-3} of SWC. The ecosystem (EC) flux was not coherent with the sum of soil and stem flux. In comparison to the high soil N$_2$O emission, the ecosystem level emission was about 5.9 times lower. Photochemical reactions and dissolution in atmospheric water are potential mechanisms by which soil-emitted N$_2$O is consumed in the forest canopies. Our results suggest that the reported N$_2$O emissions from temperate drained forests on organic soils have been greatly overestimated.

In the next decades, we anticipate a global increase in the frequency of disturbances causing hot moments of GHG emissions in terrestrial ecosystems. Our study reveals the importance of high-frequency ecosystem-scale field measurements across the year in order to accurately quantify forest GHG emissions. Full understanding of nitrogen budgets of riparian forests cannot rely only on soil level measurements but must be combined with tree-stem, canopy, and ecosystem-level EC fluxes.

METHODS

Study site and set-up

The studied hemiboreal riparian forest is a 40-year old *Filipendula* type gray alder (*Alnus incana* (L.) Moench) forest stand grown on a former agricultural land. It is situated in the Agali Village (58°17′N; 27°17′E) in eastern Estonia within the Lake Peipsi Lowland[50] (Supplementary Figs. 12 and 13).

The area is characterized by a flat relief with an average elevation of 32 m a.s.l., formed from the bottom of former periglacial lake systems, it is slightly inclined (1%) towards a tributary of the Kalli River. The soil is Gleyic Luvisol. The thickness of the humus layer was 15–20 cm. The content of total carbon (TC), total nitrogen (TN), nitrate (NO$_3^-$–N), ammonia NH$_4^+$–N, Ca, and Mg per dry matter in 10 cm topsoil was 3.8 and 0.33%, and 2.42, 2.89, 1487 and 283 mg kg^{-1}, respectively, which was correspondingly 6.3, 8.3, 4.4, 3.6, 2.3, and 2.0 times more than those in 20 cm deep zone (Supplementary Table 3).

The long-term average annual precipitation of the region is 650 mm, and the average temperature is 17.0 °C in July and –6.7 °C in January. The duration of the growing season is typically 175–180 days from mid-April to October[51].

The mean height of the forest stand is 17.5 m, stand density 1520 trees per ha, the mean stem diameter at breast height 15.6 cm, basal area 30.5 m^2 ha^{-1}, the growing stock 245 m^3 ha^{-1}, and the current annual increment of stems 12.0 m^3 ha^{-1} year^{-1} (based on Uri et al.[52] and Becker et al.[53]). In the forest floor, the following herbs dominate: *Filipendula*

ulmaria (L.) Maxim., *Aegopodium podagraria* L., *Cirsium oleraceum* (L.) Scop., *Geum rivale* L., *Crepis paludosa* (L.) Moench, shrubs (*Rubus idaeus* L., *Frangula alnus* L., *Daphne mezereum* L.), and young trees (*A. incana*, *Prunus padus* (L.)) dominate. In the moss-layer *Climacium dendroides* (Hedw.) F. Weber & D. Mohr, *Plagiomnium* spp and *Rhytidiadelphus triquetrus* (Hedw.) Warnst are overwhelming.

Environmental characteristics of hot moments

Based on high emissions of N$_2$O, dynamics of SWC, and near-ground air temperature, we identified four hot moments and related them to soil and environmental variables (see numbers in Fig. 1): wet (1), dry (2) with drought onset (2a), freeze-thaw (3), and dry-minor (4). The main criterion for the hot moments was a rapid increase in N$_2$O emissions of any source.

Anomalies from the mean of each hot moment period illustrate the pattern of fluxes during the hot moments (Supplementary Fig. 2). At the end of the freeze-thaw period, the rising SWC is driven by snowmelt became a leading determinant (Supplementary Fig. 2). During the wet period, the rise in soil emissions was accompanied by a remarkable increase in the EC-based ecosystem fluxes. However, all the other hot moments were isolated to soil surfaces.

Soil flux measurements

Soil fluxes were measured using 12 automatic dynamic chambers located at 1–2 m distance from each studied tree and installed in June 2017 (Supplementary Fig. 11, see also[54]). The chambers were made from polymethyl methacrylate (Plexiglas) covered with non-transparent plastic film. Each soil chamber (volume of 0.032 m^3) covered a 0.16 m^2 soil surface. To avoid stratification of gas inside the chamber, air with a constant flow rate of 1.8 L min^{-1} was circulated within a closed loop between the chamber and gas analyzer unit during the measurements by a diaphragm pump. The air sample was taken from the top of the chamber headspace and pumped back by distributing it to each side of the chamber. For the measurements, the soil chambers were closed automatically for 9 min each. The flushing time of the whole system with ambient air between measurement periods was 1 min. Thus, there were ~12 measurements per chamber per day, making a total of 144 flux measurements per day. A Picarro G2508 (Picarro Inc., Santa Clara, CA, USA) gas analyzer using cavity ring-down spectroscopy (CRDS) technology was used to monitor N$_2$O gas concentrations in the frequency of ~1.17 measurements per second. The chambers were connected to the gas analyzer using a multiplexer allowing a sequent practically continuous measurement.

To account for initial stabilization after chamber closing and flushing time, we used 5 min out of the total 9 min closing time (~350 concentration measurements) to estimate slope change of N$_2$O concentration, which was the basis for soil flux calculations.

After the quality check, 105,830 flux values (98.7% of total possible) of soil N$_2$O fluxes could be used during the whole study period.

Stem flux measurements

The tree stem fluxes were measured manually with frequency 1–2 times per week from September 2017 until December 2018. Twelve representative mature gray alder trees were selected for stem flux measurements and equipped with static closed tree stem chamber systems for stem flux measurements[20]. Soil fluxes were investigated close to each selected tree. The tree chambers were installed in June 2017 in the following order: at the bottom part of the tree stem (~10 cm above the soil) and at 80 and 170 cm above the ground. The rectangular shape stem chambers were made of transparent plastic containers, including removable airtight lids (Lock & Lock Co Ltd, Seoul, Republic of Korea). For the chamber, preparation see Schindler et al.[54]. Two chambers per profile were set randomly across 180° and interconnected with tubes into one system (total volume of 0.00119 m^3) covering 0.0108 m^2 of stem surface. A pump (model 1410VD, 12 V; Thomas GmbH, Fürstenfeldbruck, Germany) was used to homogenize the gas concentration prior to sampling. Chamber systems remained open between each sampling campaign. During 60 measurement campaigns, four gas samples (each 25 ml) were collected from each chamber system via septum in a 60 min interval: 0/60/120/180 min sequence (sampling time between 12:00 and 16:00) and stored in pre-evacuated (0.3 bar) 12 ml coated gas-tight vials (LabCo International, Ceregidion, UK). The gas samples were analyzed in the laboratory at the University of Tartu within a week using gas chromatography (GC-2014; Shimadzu, Kyoto, Japan) equipped with an electron capture detector for detection of N$_2$O and a flame ionization detector for CH$_4$. The gas samples

were injected automatically using Loftfield autosampler (Loftfield Analytics, Göttingen, Germany). For gas-chromatographical settings see Soosaar et al.[55].

Soil and stem flux calculation
Fluxes were quantified on a linear approach according to the change of CH_4 and N_2O concentrations in the chamber headspace over time, using the equation according to Livingston and Hutchison[56].

Stem fluxes were quantified on a linear approach according to the change of N_2O concentrations in the chamber headspace over time. A data quality control (QC) was applied based on R^2 values of linear fit for CO_2 measurements. When the R^2 value for CO_2 efflux was above 0.9, the conditions inside the chamber were applicable, and the calculations for N_2O gases were also accepted in spite of their R^2 values.

To compare the contribution of soil and stems, the stem fluxes were upscaled to hectares of ground area based on average stem diameter, tree height, stem surface area, tree density, and stand basal area estimated for each period. A cylindric shape of the tree stem was assumed. To estimate average stem emissions per tree, fitted regression curves for different periods were made between the stem emissions and height of the measurements as previously done by Schindler et al.[54].

EC instrumentation
EC system was installed on a 21 m height scaffolding tower. Fast 3-D sonic anemometer Gill HS-50 (Gill Instruments Ltd., Lymington, Hampshire, UK) was used to obtain three wind components. CO_2 fluxes were measured using the Li-Cor 7200 analyser (Li-Cor Inc., Lincoln, NE, USA). Air was sampled synchronously with the 30 m teflon inlet tube and analyzed by a quantum cascade laser absorption spectrometer (QCLAS) (Aerodyne Research Inc., Billerica, MA, USA) for N_2O concentrations. The Aerodyne QCLAS was installed in the heated and ventilated cottage near the tower base. A high-capacity free scroll vacuum pump (Agilent, Santa Clara, CA, USA) guaranteed an airflow rate of 15 L min^{-1} between the tower and gas analyzer during the measurements. Air was filtered for dust and condense water. All measurements were done at 10 Hz and the gas-analyzer reported concentrations per dry air (dry mixing ratios).

Eddy-covariance flux calculation and data QC
The fluxes of N_2O were calculated using the EddyPro software (v.6.0-7.0, Li-Cor) as a covariance of the gas mixing ratio with the vertical wind component over 30-min periods. Despiking of the raw data was performed following Mauder et al.[57]. Anemometer tilt was corrected with the double-axis rotation. Linear detrending was chosen over block averaging to minimize the influence of possible fluctuations of a gas analyzer. Time lags were detected using covariance maximization in a given time window (5 ± 2 s was chosen based on the tube length and flow rate). While Webb-Pearman-Leuning (WPL)[58] is typically performed for the closed-path systems, we did not apply it as water correction was already performed by the Aerodyne and the software reported dry mixing ratios. Both low and high-frequency spectral corrections were applied using fully analytic corrections[59,60].

Calculated fluxes were filtered out in case they were coming from the half-hour averaging periods with at least one of the following criteria: more than 1000 spikes, half-hourly averaged mixing ratio out of range (300–350 ppb), QC flags higher than 7[61].

The footprint area was estimated using Kljun et al.[62] implemented in TOVI software (Li-Cor Inc.). A footprint allocation tool was implemented to flag the non-forested areas within the 90% cumulative footprint and fluxes appointed to these areas were removed from the further analysis.

Storage fluxes were estimated using concentration measurements from the eddy system (Eq. (1)), assuming the uniform change within the air column under the tower during every 30 min period[63,64]:

$$S = \Delta C/\Delta t * z_m, \tag{1}$$

where S is storage, ΔC is change in the dry mixing ratio of N_2O, Δt is time period (30 min), z_m is measurement height (21 m).

In the absence of a better estimate or profile measurements, these estimates were used to correct for storage change. Total flux values that were higher than eight times the standard deviation were additionally filtered out (following Wang et al.[36]). Overall, the QC procedures resulted in 61% data coverage.

While friction velocity (u^*) threshold is used to filter eddy fluxes of CO_2[65], visual inspection of the friction velocity influence on N_2O fluxes demonstrated no effect. Thus, we decided not to apply it, taking into account that the 1–9 QC flag system already marks the times when the turbulence is not sufficient.

To obtain the continuous time-series and to enable the comparison to chamber estimates over hourly time scales, gap-filling of N_2O fluxes was performed using marginal distribution sampling method implemented in ReddyProcWeb online tool (https://www.bgc-jena.mpg.de/bgi/index.php/Services/REddyProcWeb) (described in detail in Wutzler et al.[66]).

MATLAB (ver. 2018a-b, Mathworks Inc., Natick, MA, USA) was used for all the eddy fluxes data analysis.

Ancillary measurements
Air temperature, relative and absolute humidity were measured within the canopy at 10 m height using the HC2A-S3—Standard Meteo Probe/RS24T (Rotronic AG, Bassersdorf, Switzerland) and Campbell CR100 data logger (Campbell Scientific Inc., Logan, UT, USA). The potential amount of dissolved N_2O in the atmospheric water was calculated based on the absolute humidity and the maximum solubility of N_2O in water[67]. DPD was calculated from air temperature and estimated dew point temperature to characterize the chance of fog formation within the canopy. The solar radiation data were obtained from the SMEAR Estonia station located at 2 km from the study site[68] using the Delta-T-SPN-1 sunshine pyranometer (Delta-T Devices Ltd., Cambridge, UK). The cloudiness ratio was calculated as the ratio of diffuse solar radiation to total solar radiation.

Near-ground air temperature, soil temperature (Campbell Scientific Inc.), and SWC sensors (ML3 ThetaProbe, Delta-T Devices, Burwell, Cambridge, UK) were installed directly on the ground and 0–10 cm soil depth close to the studied tree spots. During six campaigns from August to November 2017, composite topsoil samples were taken with a soil corer from a depth of 0–10 cm for physical and chemical analysis using standard methods[69].

Statistical analysis
R version 4.0.2 (R Development Core Team, 2020) was used to examine, analyze and visualize the data. The significance level (alpha) considered for all the tests was 0.05. The "akima" package version 0.6–2.1 was used to create interpolated contour plots representing a three-dimensional surface[70] by plotting soil temperature and SWC against soil N_2O emissions as the independent variable. Linear regression models were fitted and Spearman's rank correlation coefficients were shown for change of SWC and soil N_2O flux in period drought onset and air temperature and soil N_2O flux in period freeze-thaw. Spearman's rank correlation coefficients were also shown characterizing the relationship between the monthly average number of days with a high chance of sunshine and fog formation and the difference between the N_2O flux from soil and ecosystem. Regarding all measurements of soil temperature, SWC, and soil N_2O flux, relationships were better represented by nonlinear than linear models. In addition, the Bragg equation with four parameters[71] was used for describing the relationship between SWC and soil N_2O flux in the dry period. A workflow for the nonlinear regression analysis was used[72] and regression models were fitted in R using functions lm, nls, or loess.

REFERENCES
1. Baldocchi, D. Measuring fluxes of trace gases and energy between ecosystems and the atmosphere—the state and future of the eddy covariance method. *Glob. Chang. Biol.* 3600–3609 https://doi.org/10.1111/gcb.12649 (2014).
2. U.S. EPA. *Methane and nitrous oxide emissions from natural sources.* EPA 430-R-10-001 (2010).
3. Myhre, G. et al. Anthropogenic and natural radiative forcing. In *Climate Change 2013: The Physical Science Basis. Working Group I Contribution to the Fifth*

Assessment Report of the Intergovernmental Panel on Climate Change 659–740 (Cambridge University Press, Cambridge, UK, 2013).

4. Ravishankara, A. R., Daniel, J. S. & Portmann, R. W. Nitrous oxide (N_2O): the dominant ozone depleting substance emitted in the 21st century. *Science* **326**, 123–125 (2009).

5. Butterbach-Bahl, K., Baggs, E. M., Dannenmann, M., Kiese, R. & Zechmeister-Boltenstern, S. Nitrous oxide emissions from soils: how well do we understand the processes and their controls? *Philos. Trans. R. Soc. B Biol. Sci.* **368**, 20130122 (2013).

6. Mander, Ü. et al. Isotopologue ratios of N_2O and N_2 measurements underpin the importance of denitrification in differently N-loaded riparian alder forests. *Environ. Sci. Technol.* **48**, 11910–11918 (2014).

7. Hagedorn, F. & Bellamy, P. Hot spots and hot moments for greenhouse gas emissions from soils. In *Soil Carbon in Sensitive European Ecosystems: From Science to Land Management* (eds. Jandl, R., Rodeghiero M. & Olsson, M.) 13–32. (Blackwell Science Publication, Oxford, UK, 2011).

8. Christiansen, J. R., Vesterdal, L. & Gundersen, P. Nitrous oxide and methane exchange in two small temperate forest catchments—effects of hydrological gradients and implications for global warming potentials of forest soils. *Biogeochemistry* **107**, 437–454 (2011).

9. Pärn, J. et al. Nitrogen-rich organic soils under warm well-drained conditions are global nitrous oxide emission hotspots. *Nat. Commun.* **9**, 1–8 (2018).

10. Liengaard, L. et al. Hot moments of N_2O transformation and emission in tropical soils from the Pantanal and the Amazon (Brazil). *Soil Biol. Biochem.* **75**, 26–36 (2014).

11. Goldberg, S. D. & Gebauer, G. N_2O and NO fluxes between a Norway spruce forest soil and atmosphere as affected by prolonged summer drought. *Soil Biol. Biochem.* **41**, 1986–1995 (2009).

12. Teepe, R., Vor, A., Beese, F. & Ludwig, B. Emissions of N_2O from soils during cycles of freezing and thawing and the effects of soil water, texture and duration of freezing. *Eur. J. Soil Sci.* **55**, 357–365 (2004).

13. Groffman, P., Hardy, J., Driscoll, C. T. & Fahey, T. J. Snow depth, soil freezing, and fluxes of carbon dioxide, nitrous oxide and methane in a northern hardwood forest. *Glob. Change Biol.* **12**, 1748–1760 (2006).

14. Chen, L. X. et al. Influences of forest cover on soil freeze-thaw dynamics and greenhouse gas emissions through the regulation of snow regimes: a comparison study of the farmland and forest plantation. *Sci. Total Environ.* **726**, 138403 (2020).

15. Viru, B. et al. Wintertime greenhouse gas fluxes from hemiboreal drained peatlands. *Atmosphere* **11**, 731 (2020).

16. Teepe, R., Brumme, R. & Beese, F. Nitrous oxide emissions from soil during freezing and thawing periods. *Soil Biol. Biochem.* **33**, 1269–1275 (2001).

17. Groffman, P. M. et al. Colder soils in a warmer world: a snow manipulation study in a northern hardwood forest ecosystem. *Biogeochemistry* **56**, 135–150 (2001).

18. Pihlatie, M., Ambus, P., Rinne, J., Pilegaard, K. & Vesala, T. Plant-mediated nitrous oxide emissions from beech (*Fagus sylvatica*) leaves. *New Phytol.* **168**, 93–98 (2005).

19. Machacova, K. et al. *Pinus sylvestris* as a missing source of nitrous oxide and methane in boreal forest. *Sci. Rep.* **6**, 1–8 (2016).

20. Machacova, K., Vainio, E., Urban, O. & Pihlatie, M. Seasonal dynamics of stem N_2O exchange follow the physiological activity of boreal trees. *Nat. Commun.* **10**, 1–13 (2019).

21. Vargas, R. & Barba, J. Greenhouse gas fluxes from tree stems. *Trends Plant Sci.* **24**, 296–299 (2019).

22. Caudullo, G., Welk, E. & San-Miguel-Ayanz, J. Chorological maps for the main European woody species. *Data Brief.* **12**, 662–666 (2017).

23. Pihlatie, M. et al. Nitrous oxide emissions from a beech forest floor measured by eddy covariance and soil enclosure techniques. *Biogeosciences* **2**, 377–387 (2005).

24. Eugster, W. et al. Methodical study of nitrous oxide eddy covariance measurements using quantum cascade laser spectrometry over a Swiss forest. *Biogeosciences* **4**, 927–939 (2007).

25. Nemitz, E. et al. Standardisation of eddy-covariance flux measurements of methane and nitrous oxide. *Int. Agrophys.* **32**, 517–549 (2018).

26. Barrat, H. A. et al. The impact of drought and rewetting on N_2O emissions from soil in temperate and Mediterranean climates. *Eur. J. Soil Sci.* 1–13 https://doi.org/10.1111/ejss.13015 (2020).

27. Petrakis, S., Seyfferth, A., Kan, J. J., Inamdar, S. & Vargas, R. Influence of experimental extreme water pulses on greenhouse gas emissions from soils. *Biogeochemistry* **133**, 147–164 (2017).

28. Mander, Ü. et al. The impact of a pulsing groundwater table on greenhouse gas emissions in riparian grey alder stands. *Environ. Sci. Pollut. Res.* **22**, 2360–2371 (2015).

29. Von Arnold, K., Weslien, P., Nilsson, M., Svensson, B. H. & Klemedtsson, L. Fluxes of CO_2, CH_4 and N_2O from drained coniferous forests on organic soils. *For. Ecol. Manag.* **210**, 239–254 (2005).

30. Kim, D.-G., Vargas, R., Bond-Lamberty, B. & Turetsky, M. R. Effects of soil rewetting and thawing on soil gas fluxes: a review of current literature and suggestions for future research. *Biogeosciences* **9**, 2459–2483 (2012).

31. Öquist, M. G. et al. Nitrous oxide production in a forest soil at low temperatures—processes and environmental controls. *FEMS Microbiol. Ecol.* **49**, 371–378 (2004).

32. Kaushal, S. S. et al. Watershed 'chemical cocktails': forming novel elemental combinations in Anthropocene fresh waters. *Biogeochemistry* **141**, 281–305 (2018).

33. Schimel, J. P. Life in dry soils: effects of drought on soil microbial communities and processes. *Annu. Rev. Ecol. Evol. Syst.* **49**, 409–432 (2018).

34. Gillespie, L. M. et al. Higher tree diversity increases soil microbial resistance to drought. *Commun. Biol.* **3**, 377 (2020).

35. Shurpali et al. Neglecting diurnal variations leads to uncertainties in terrestrial nitrous oxide emissions. *Sci. Rep.* **6**, 25739 (2016).

36. Wang, J. M. et al. Methane fluxes measured by eddy covariance and static chamber techniques at a temperate forest in central Ontario, Canada. *Biogeosciences* **10**, 4371–4382 (2013).

37. Bao, T. et al. Potential effects of ultraviolet radiation reduction on tundra nitrous oxide and methane fluxes in maritime Antarctica. *Sci. Rep.* **8**, 3716 (2018).

38. Prather, M. J. et al. Measuring and modeling the lifetime of nitrous oxide including its variability. *J. Geophys. Res. Atmos.* **120**, 5693–5705 (2015).

39. Fraser, W. T. et al. UV-B absorbing pigments in spores: biochemical responses to shade in a high-latitude birch forest and implications for sporopollenin-based proxies of past environmental change. *Polar Res.* **30**, 8312 (2011).

40. Kuusk, J. & Kuusk, A. Hyperspectral radiometer for automated measurement of global and diffuse sky irradiance. *J. Quant. Specrosc. Radiat. Trans.* **204**, 272–280 (2018).

41. Dowdell, R. J., Burford, J. R. & Crees, R. Losses of nitrous oxide dissolved in drainage water from agricultural land. *Nature* **278**, 342–343 (1979).

42. Warneke, S., Macdonald, B. C. T., Macdonald, L. M., Sanderman, J. & Farrell, M. Abiotic dissolution and biological uptake of nitrous oxide in Mediterranean woodland and pasture soil. *Soil Biol. Biochem.* **82**, 62–64 (2015). 2015.

43. Min, K.-E. et al. Eddy covariance fluxes and vertical concentration gradient measurements of NO and NO_2 over a ponderosa pine ecosystem: observational evidence for within-canopy chemical removal of NOx. *Atmos. Chem. Phys.* **14**, 5495–5512 (2014).

44. Fulgham, S. R. et al. Surface wetness as an unexpected control on forest exchange of volatile organic acids. *Geophys. Res. Lett.* **47**, e2020GL088745 (2020).

45. Kram, K. J. Modification of the atmospheric load of elements during passage through foliaged canopies of five tree species of temperate zone forests. *Pol. J. Ecol.* **58**, 87–101 (2010).

46. Rebmann, C. et al. ICOS eddy covariance flux-station site setup: a review. *Int. Agrophys.* **32**, 471–494 (2018).

47. IPCC. *Supplement to the 2006 IPCC Guidelines for National Greenhouse Gas Inventories: Wetlands.* (eds Hiraishi, T. et al). (IPCC, Switzerland, 2013).

48. Saikawa, E. et al. Global and regional emissions estimates for N_2O. *Atmos. Chem. Phys.* **14**, 4617–4641 (2014).

49. Clerici, N. et al. Pan-European distribution modelling of stream riparian zones based on multi-source earth observation data. *Ecol. Indic.* **24**, 211–223 (2013).

50. Varep, E. The landscape regions of Estonia. Publications on geography IV. *Acta Comm. Univ Tartuensis* **156**, 3–28 (1964).

51. Kupper, P. et al. An experimental facility for free air humidity manipulation (FAHM) can alter water flux through deciduous tree canopy. *Environ. Exp. Bot.* **72**, 432–438 (2011).

52. Uri, V. et al. The dynamics of biomass production, carbon and nitrogen accumulation in grey alder (*Alnus incana* (L.) Moench) chronosequence stands in Estonia. *For. Ecol. Manag.* **327**, 106–117 (2014).

53. Becker, H. et al. The effects of clear-cut on net nitrogen mineralization and nitrogen losses in a grey alder stand. *Ecol. Eng.* **85**, 237–246 (2015).

54. Schindler, T. et al. Short-term flooding increases CH_4 and N_2O emissions from trees in a riparian forest soil-stem continuum. *Sci. Rep.* **10**, 3204 (2020).

55. Soosaar, K. et al. Dynamics of gaseous nitrogen and carbon fluxes in riparian alder forests. *Ecol. Eng.* **37**, 40–53 (2011).

56. Livingston, G. P. & Hutchinson, G. L. Enclosure-based measurement of trace gas exchange: applications and sources of error. In *Biogenic Trace Gases: Measuring Emissions from Soil and Water* (eds. Matson, P. A. & Harriss, R. C.) 14–51 (Ed. Blackwell Publishing: Oxford, UK, 1995).

57. Mauder, M. et al. A strategy for quality and uncertainty assessment of long-term eddy-covariance measurements. *Agr. For. Meteorol.* **169**, 122–135 (2013).

58. Webb, E. K., Pearman, G. I. & Leuning, R. Correction of flux measurements for density effects due to heat and water vapour transfer. *Quart. J. R. Met. Soc.* **106**, 85–100 (1980).

59. Moncrieff, J. B. et al. A system to measure surface fluxes of momentum, sensible heat, water vapor and carbon dioxide. *J. Hydrol.* **188-189**, 589–611 (1997).

60. Moncrieff, J. B., Clement, R., Finnigan, J. & Meyers T. Averaging, detrending and filtering of eddy covariance time series. In *Handbook of Micrometeorology: A Guide for Surface Flux Measurements* (eds. Lee, X., W. J. Massman & Law, B. E.) 7–31 (Kluwer Academic, Dordrecht, 2004).

61. Foken, T., Göockede, M., & Mauder, M. Post-field data quality control. In *Handbook of Micrometeorology: a Guide for Surface Flux Analysis* (eds. Lee, X. H., Massman, W. & Law, B.) 181–208. Issue 1988 (2004).

62. Kljun, N., Calanca, P., Rotach, M. W. & Schmid, H. P. A simple two-dimensional parameterisation for flux footprint prediction (FFP). *Geosci. Model Dev.* **8**, 3695–3713 (2015).

63. Hollinger, D. Y. et al. Carbon 'dioxide exchange between an undisturbed old-growth temperate forest and the atmosphere. *Ecology* **7**, 134–150 (1994).

64. Greco, S. & Baldocchi, D. B. Seasonal variations of CO_2 and water vapour exchange rates over a temperate deciduous forest. *Glob. Change Biol.* 2, 183–197 (1996).

65. Papale, D. et al. Towards a standardized processing of net ecosystem exchange measured with eddy covariance technique: algorithms and uncertainty estimation. *Biogeosciences* **3**, 571–583 (2006).

66. Wutzler, T. et al. Basic and extensible post-processing of eddy covariance flux data with REddyProc. *Biogeosci. Discuss.* 1–39 (2018).

67. Jenni, S., Mohn, J., Emmenegger, L. & Udert, K. M. Temperature dependence and interferences of NO and N_2O microelectrodes used in wastewater treatment. *Environ. Sci. Technol.* **46**, 2257–2266 (2012). 2012.

68. Noe, S. M. et al. SMEAR Estonia: perspectives of a large-scale ecosystem-atmosphere research infrastructure. *Forestry Stud.* **63**, 66–84 (2015).

69. APHA-AWWA-WEF. *Standard Methods for the Examination of Water and Wastewater*, 21th ed. (American Public Health Organisation, 2005).

70. Akima, H., Gebhardt, A., Petzold, T., & Maechler, M. *Akima: Interpolation of Irregularly and Regularly Spaced Data. R Package Version 0.6-2.1.* (2016). https://cran.r-project.org/web/packages/akima/index.html Accessed 06 Aug 2020.

71. Ratkwosky, D. A. *Handbook of Nonlinear Regression Models (No. 04; QA278. 2, R3.)* 241 (M. Dekker, New York, USA, 1990).

72. Archontoulis, S. V. & Miguez, F. E. Nonlinear regression models and applications in agricultural research. *Agron. J.* **107**, 786–798 (2015).

ACKNOWLEDGEMENTS

AUTHOR CONTRIBUTIONS

Ü.M., K.S., K.M., and Ü.N. designed this study, Ü.M., K.S., A.K., J.P., M.E., J.E.G., T.S., M.P., and P.M. wrote the paper, T.S., M.M., K.S., and Ü.M. conducted the field work, Ü.M., K.S., A.K., M.E., J.E.G., and K.M. carried out data checks and analysis, J.P. deposited the data, and all authors commented on the paper.

COMPETING INTERESTS

The authors declare no competing interests.

ADDITIONAL INFORMATION

Supplementary information The online version contains supplementary material available at https://doi.org/10.1038/s41612-021-00194-7.

Correspondence and requests for materials should be addressed to Ü.M.

Reprints and permission information is available at http://www.nature.com/reprints

Publisher's note Springer Nature remains neutral with regard to jurisdictional claims in published maps and institutional affiliations.